Technical Note

Overflow of Dual Parapet Walls on Dam Crests

Hubert Chanson[1]

Abstract: To facilitate service vehicle access, dam and weir crests and spillways are often constructed with a flat crest. Parapet walls are often included on the upstream and downstream sides for safety. In such cases, it is sometimes assumed that the resulting structure performs like a broad-crested weir, as though the fluid between the parapet walls is stagnant and has the same effect on the overflow as a solid crest. Physical measurements were undertaken to test the effects of dual-parapet walls with three configurations: a reference flat weir without parapet wall and two configurations with dual-parapet walls. The experiments showed some markedly different flow patterns above the weir crest in presence of parapet walls. The water trapped between the parapet walls behaved as a recirculating pool, and this affected the flow over the weir and the head–discharge relationship. With increasing relative discharges, the flow pattern above the weir crest evolved from plunge flow over the first parapet wall to undular, then breaking, and later deflected, before achieving the flow characteristics of a thick-crested weir at the largest discharges. Quantitative measurements also highlighted some large energy dissipation. The discharge coefficient was smaller in presence of parapet walls, with a reduction of 7% to 12% in the discharge capacity compared with that of a broad-crested weir. **DOI: 10.1061/JIDEDH.IRENG-10549.**

Author keywords: Broad-crested weirs; Parapet walls; Physical modeling; Discharge characteristics; Hydraulic structures; Spillways; Dam crest.

Introduction

Dams and reservoirs are human-made infrastructure, intended to store water and mitigate the impact of runoff, and they must be equipped with a spillway system (USBR 1965; Novak et al. 1996). At an overflow spillway, the spillway capacity is linked to the crest design shape (Ackers et al. 1978; Chanson 2004). Rounded crest weirs can have larger discharge coefficients, but the broad crest design is simple to develop and to build, and the wider crest may facilitate vehicular access across the weir crest during construction and during the lifetime of the structure. Practically, the dimensionless crest length $L/(H_1 - P)$ should be larger than 1.5 to 3, with H_1 the upstream total head, P the weir crest elevation, and L the weir crest length (Govinda Rao and Muralidhar 1963; Henderson 1966) [Fig. 1(a)].

The unit discharge q above a weir crest is typically expressed

$$q = C_D \times \sqrt{g \times \left(\frac{2}{3} \times (H_1 - P)\right)^3} \tag{1}$$

where C_D = dimensionless discharge coefficient; and g = gravity acceleration. The discharge coefficient C_D is typically slightly less than unity, and it is a function of the weir height, crest length, crest width, upstream corner shape, and upstream total head (Bos 1976; Ackers et al. 1978).

In Australia, a number of large dams were equipped with secondary and tertiary spillways with a flat crest and dual-parapet walls. Fig. 2 presents a couple of examples of flat-crest designs equipped with concrete parapet walls on the upstream and downstream sides. In each case, the dam crest with dual-parapet walls was designed to be overtopped during large to major flood events. The dual-parapet walls were included for occupational health and safety (OH&S) and serviceability and are essential features for the safety of the operators.

To date, the discharge rating curves of the spillways equipped with a flat crest and dual parapet walls were assumed to be that of a broad-crested weir with the invert set at the top of the parapet walls. The present study was motivated by the knowledge gap on the effects of parapet walls on the overflow and operation. The aim of the research project was a characterization of the effects of dual-parapet walls, with a systematic comparison with a reference broad-crested weir without parapet wall. Detailed visual observations and hydraulic measurements were made in physical model tests to compare the hydraulic performance.

Physical Modeling and Experimental Setup

Physical experiments are commonly used to study the performance of hydraulic structures, and a Froude similitude is typically used to preserve the ratio of fluid inertia and gravitational forces. In small-size models, however, viscous scale effects might take place because the Reynolds number is significantly smaller than at full-scale (Chanson 2004; Novak et al. 2010). Herein, a Froude similitude was applied, and the physical experiments were undertaken in relatively large size facilities, thus ensuring optimum model-prototype compliance.

New physical experiments were conducted in two flumes in the advanced engineering building (AEB) Hydraulics Laboratory at the University of Queensland (Fig. 1). The flumes were identical except for the discharge measurement technique. In each flume, the water was supplied to a 1.0-m-deep, 0.90-m-wide, and 0.75-m-long intake basin, followed by a three-dimensional convergent section, 0.55 m long with a 2.25:1 contraction ratio, resulting in a smooth and waveless flow in the 0.4-m-wide test section. Each test section was 3 m long. The invert was horizontal and made of PVC. The sidewalls were 0.40 m high and made of transparent glass. The broad-crested

[1]Professor in Hydraulic Engineering, School of Civil Engineering, Univ. of Queensland, Brisbane, QLD 4072, Australia. ORCID: https://orcid.org/0000-0002-2016-9650. Email: h.chanson@uq.edu.au

Note. This manuscript was submitted on December 16, 2024; approved on January 29, 2025; published online on April 2, 2025. Discussion period open until September 2, 2025; separate discussions must be submitted for individual papers. This technical note is part of the ***Journal of Irrigation and Drainage Engineering***, © ASCE, ISSN 0733-9437.

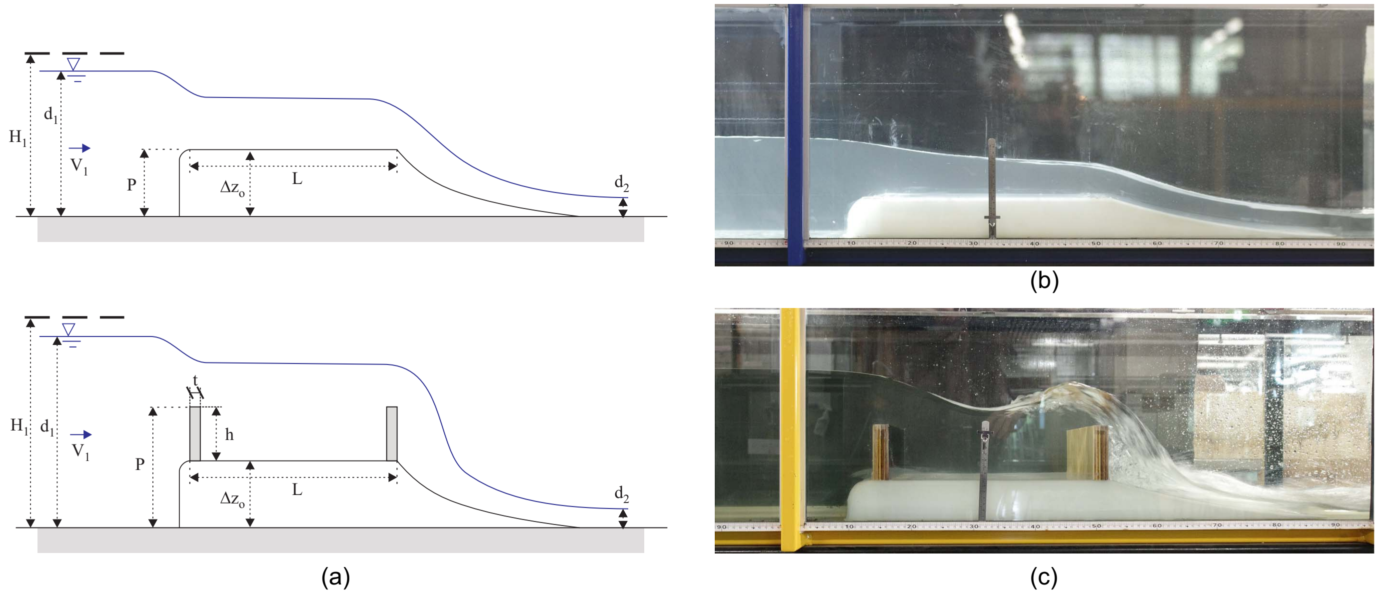

Fig. 1. Reference broad-crested weir and broad-crested weir with dual-parapet walls: (a) definition sketches of reference broad-crested weir and broad-crested weir with dual-parapet walls; (b) reference broad-crested weir with flow direction from left to right and $d_c/L = 0.173$; and (c) broad-crested weir with dual-parapet walls (Configuration I) with flow direction from left to right and $d_c/L = 0.145$, deflected jet flow pattern.

weir was installed 1.13 m downstream from the start of the glass-sidewall test section, which ended with an overfall, guiding the supercritical outflow.

The water was supplied by a constant-head delivery system, allowing a constant water discharge over long periods of time. In Flume A, the water discharge was measured with an orifice meter installed in the delivery pipeline and built based upon British Standard Institution (BSI) guidelines (BSI 1943) and calibrated in situ against a large V-notch weir. In Flume B, the flow rate was measured with a 90° V-notch weir, calibrated independently with flow rates up to 0.12 m^3/s (Chanson and Wang 2013). The water depths were measured with rail-mounted pointer gauges, with verniers marked in gradations of 0.2 mm, as well as through the glass sidewalls. Visual observations were also recorded with an Apple (Cupertino, California) iPhone XI and a digital single lens reflex (dSLR) Pentax (Tokyo) K-3iii camera equipped with professional-grade prime lenses with negligible lens distortion.

Three dam crest configurations were tested (Table 1). The reference broad-crest geometry had a vertical upstream wall, an upstream rounded corner ($r = 30$ mm), and a 0.39-m-long horizontal crest, followed by a smooth downstream slope [Fig. 1(b)]. The sill crest was 0.066 m above the PVC invert, and the broad-crested weir structure was made out of polymethyl methacrylate. The other two configurations represented a broad crest geometry topped with two identical parapet walls, installed on the upstream and downstream edges of the reference broad-crested weir [Figs. 2(a and c)]. For Configuration I, the parapet walls were 0.157 m high and 0.025 m thick. For Configuration II, the dual-parapet walls were 0.187 m high and 0.033 m thick. The walls were made of marine ply, machine cut with ±0.25-mm tolerance, and impervious. The experimental Configuration II corresponded to a 1:13 scale study of the spillway crest design shown in Fig. 2(b). The two geometries could be installed in Flumes A or B indiscriminately.

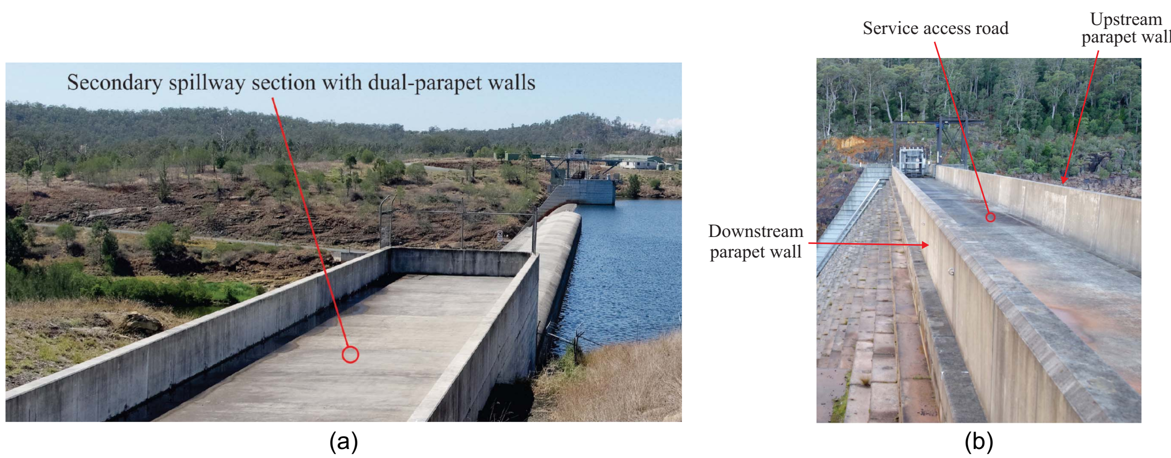

Fig. 2. Broad-crested weirs with parapet walls: (a) Wyaralong Dam (Australia) on October 2, 2021, with secondary spillway section with dual-parapet walls, with the right bank in the background; and (b) Meander Dam (Australia) on May 29, 2023, with tertiary spillway with dual-parapet walls, with the right bank in the background. (Images by author.)

Table 1. Experimental flow conditions of broad-crested weir study without and with dual-parapet walls

Weir type	B (m)	L (m)	Δz_o (m)	h (m)	P (m)	t (m)	Q (m^3/s)	Weir geometry	d_c/L	Re	Comment
Reference	0.4	0.392	0.066	—	0.065	—	0.0009 to 0.023	Rounded edge and solid-lid crest	0.02 to 0.10	0.6×10^4 to 0.6×10^5	No parapet wall ($r = 30$ mm)
Configuration I	0.4	0.387	0.066	0.091	0.157	0.025	0.003 to 0.057	Rounded edge and parapet walls	0.043 to 0.33	1.4×10^4 to 2.0×10^5	Parapet walls
Configuration II	0.4	0.392	0.066	0.121	0.187	0.033	0.0012 to 0.042	Rounded edge and parapet walls	0.025 to 0.27	0.4×10^4 to 1.5×10^5	Parapet walls

Note: B = channel breadth; d_c = critical flow depth; h = vertical parapet wall height; L = broad-crest length; P = crest height, where $P = \Delta z_o + h$; Q = water discharge; Re = Reynolds number defined in terms of the hydraulic diameter D_H; t = parapet wall thickness; and Δz_o = weir crest height. A dash indicates that the information is not relevant.

The experimental observations were conducted for water discharges between 0.0009 and 0.057 m^3/s, corresponding to dimensionless discharges d_c/L between 0.02 and 0.33 and Reynolds numbers up to 2.0×10^5, where d_c is the critical depth (Table 1). The ratio $d_c/L = q^{2/3}/(g^{1/3} \times L)$, and thus it represents a dimensionless unit discharge defined in terms of the crest length. Table 1 lists the details of the experimental configurations and flow conditions.

The experiments were performed with increasing and decreasing discharges to test for hysteresis, such as that previously reported at circular-crested weirs (Chanson 2024). No hysteresis was observed in the head–discharge relationship nor any effect of the rate of change of flow rate on the steady flow data. Further, the submergence of the weir or parapet walls by downstream tailwater was not considered.

Flow Patterns

Overtopping Flow

For the reference broad-crested weir, the upstream flow was subcritical and slow. The fluid accelerated over the broad crest and became supercritical and fast-flowing on the downstream smooth steep slope [Fig. 1(b)]. For very low flow, with unit discharges $q < 0.016$ m^2/s and $d_c/L < 0.076$, the free surface over the weir crest was undular (Chanson 1995, 1996). The flow above the crest was further affected by a developing boundary layer (Isaacs 1981). For $0.076 < d_c/L < 0.2$, the streamlines were quasi-parallel to the crest, and the pressure distribution was hydrostatic above the crest, as inferred from the observations of quasi-horizontal streamlines. Small corner vortices were seen next to the sidewalls and invert next to the upstream end of the weir. Although similar spiral eddies were illustrated by Rouse (1938, pp. 75, 271), the present weir geometry was relatively short ($P/L = 0.17$), and the effects of the corner vortices on the broad-crested weir overflow were negligible, in contrast to earlier studies of tall broad-crested weirs, e.g., those of Gonzalez and Chanson (2007) and Zhang and Chanson (2016). For larger discharges, the reference broad-crested weir acted as a thick-crested weir, and the streamlines were no longer parallel to the crest invert, implying that the pressure distributions were not hydrostatic.

With the addition of dual-parapet walls, the flow upstream from the structure remained tranquil and slow (subcritical) but the parapet walls dramatically changed the flow region between the two walls, acting as a recirculation cell. The type of recirculation pattern was a function of the relative discharge d_c/L and weir geometry. Several photographs are presented in Fig. 3, and a number of video movies are available, as described in the Appendix.

A chart identifying operating zones for the different flow patterns is presented in Fig. 4. The addition of the dual-parapet walls caused the structure to no longer behave like a simple, rigid, flat-topped broad-crested weir. Instead, the flow over dual-parapet walls presented a number of markedly distinctive flow patterns depending upon the dimensionless discharge d_c/L. Most flow patterns were common to both Configurations I and II, i.e., $L/h = 4.3$ and 3.2, respectively, with h being the parapet wall height. At very low flow rates, the flow was critical over the upstream parapet wall and subcritical between the two parapet walls. The upstream wall acted as a thick-crested weir. Although these flow conditions were not investigated in depth because of the very small change in depths over the upstream parapet wall, two distinct flow patterns might be envisaged. At the very lowest flow, the jet might plunge over the first parapet wall and remain attached to the downstream side of the

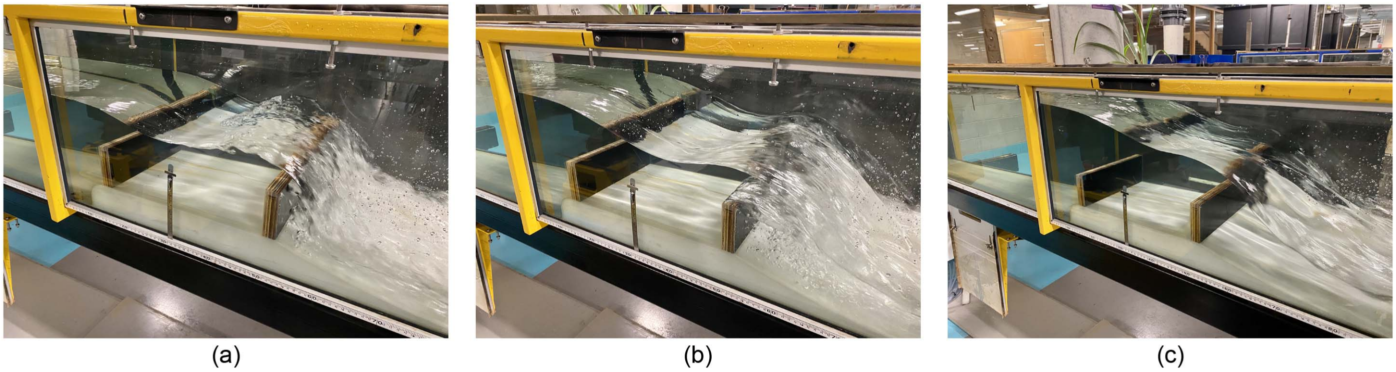

Fig. 3. Overflow above broad-crested weir with dual-parapet walls in Configuration I: (a) oscillating jump between parapet walls, $d_c/L = 0.145$, $L/h = 4.3$; (b) deflected jet above downstream parapet wall, $d_c/L = 0.221$, $L/h = 4.3$; and (c) thick-crested weir overflow, $d_c/L = 0.312$, $L/h = 4.3$.

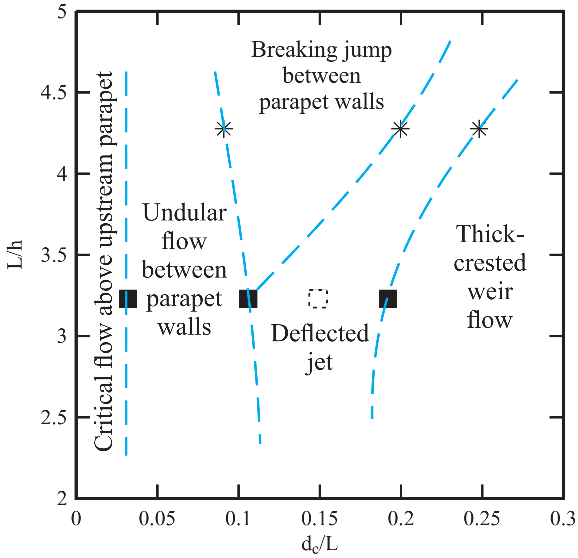

Fig. 4. Flow regimes above broad-crested weirs with dual-parapet walls: present study, Configurations I and II.

wall. At higher flow rates, the jet could detach from the upstream parapet wall and induce a plunge into the pool between the parapet walls.

With increasing discharge, the water surface was undular between the parapet walls. Visually, the free surface presented similarities with undular flows downstream of backward-facing steps and submerged bodies (Duncan 1983; Chanson 1996). In the present study, the location of the undulation start shifted downstream, and the number of secondary waves decreased with increasing discharges. The videos IMGP5631.mov and IMGP5222.mov (Supplemental Materials) show two side views of the water surface profile for $d_c/L = 0.085$ and 0.068 with Configurations I and II, respectively. In each movie, the injection of red dye highlights the recirculation cell in the cavity beneath the secondary undulations.

In Configuration I (i.e., $L/h = 4.3$), the undular flow transformed into a breaking, oscillating jump near the downstream end of the crest [Fig. 3(a)] for a relatively narrow range of discharges before the jet became deflected over the downstream parapet wall at larger discharges. The oscillating jump moved back and forth between the parapet walls, and these longitudinal oscillations were associated with relatively large fluctuations of the upstream water levels, with amplitudes up to ±2 mm in the physical model. The jump roller is alternately breaking and then swept further downstream, oscillating back and forth.

The movies IMGP4738.mov and IMG_1826.mov in the Supplemental Materials illustrate the oscillating motion of the breaking roller for $d_c/L = 0.164$ with Configuration I. The first movie shows a side view of the overflow, highlighting the strong surface deformation associated with wave breaking and some limited air bubble entrainment in the roller between the parapet walls. The fluctuations in upstream water levels are seen on the left of the video movie. The second movie presents a top view of the breaking of the roller, with flow direction from left to right. The video illustrates the complicated three-dimensional breaking motion, as well as the relatively large longitudinal shifts in roller toe position, typical of oscillating hydraulic jumps (Mossa 1999).

For larger discharges, the water was rapidly accelerated as it passed over the upstream parapet wall, and the flow was deflected upward as it passed over the downstream parapet wall [Fig. 3(b)]. An air cavity formed immediately downstream of the second parapet wall, and substantial energy dissipation was observed at jet impact onto the downstream slope of the weir. The video movies IMGP5641.mov and IMGP5550.mov (Supplemental Materials) present some side views of the deflected jet flow with Configurations I and II, respectively.

For the largest discharges, the flow pattern became similar to a skimming flow regime, also called quasi-smooth or tranquil flow (Morris 1968; Chanson 1994). Visually, the entire structure acted in aggregate as a thick-crested weir (Bresse 1868), and the influence of the parapet walls could only be seen through the transparent sidewalls [Fig. 3(c)]. The movie IMGP5173.mov (Supplemental Materials) illustrates an example of such a flow motion.

For Configurations I and II, the present observations of the changes in flow regimes are summarized in Fig. 4, which shows regions of each flow regime in relation to the characteristic dimensionless discharge d_c/L and the ratio L/h of crest length to parapet wall height. In absence of parapet walls, i.e., $L/h \to +\infty$, the flow regimes are undular, broad-crested weir, and thick-crested weir flows only.

Flow Recirculation

With dual-parapet walls in place, dye injection observations showed the presence of strong recirculation between the parapet walls at all dimensionless flow rates. During the overflow, the recirculation developed between the walls and the motion followed a complicated three-dimensional pattern, which was a function of flow regime and relative discharge d_c/L. For the smaller flow rates, the recirculating eddies between parapets walls were similar to dangerous recirculation conditions seen below low-head dams and weirs (Leutheusser and Birk 1991; Hotchkiss 2001). The recirculation can produce currents that trap swimmers, boaters, and potential rescuers. For the larger discharges, there was some similarity with the recirculatory patterns described in open-channel flow past strip roughness (Morris 1968) and past rectangular cavities (Lin and Rockwell 2001) with comparable cavity aspect ratio L/h.

In the current study, the recirculation was mostly documented through sidewall photographs and video movies with dye injection (Supplemental Materials). The movies IMGP5631.mov, IMGP5641.mov, IMGP5522.mov, and IMGP5550.mov present side view recordings of dye injection next to the sill crest between the parapet walls. They illustrate the recirculation beneath the main flow stream. Visual, photographic, and cinematographic observations showed conclusively that the overflow motion above a broad-crested weir with parapet walls differed from the flow over a flat, rigid-topped, broad-crested weir [e.g., Fig. 1(b)].

Discharge Characteristics

Quantitative measurements were performed for a wide range of flow conditions, with both increasing and decreasing discharges. No hysteresis was observed, and the results were identical for a given discharge, whether the flow rate was increased or decreased. The data sets for the upstream water depth are reported in Fig. 5(a) for all three configurations (Table 1). The graph showed a monotonic increase in water depths with increasing discharges.

In Fig. 5(a), the $1.5V{:}1H$ slope was added for comparison because the $1.5V{:}1H$ slope would mean $(d_1 - P) = 3/2 \times d_c$. The present data indicated a slightly different slope between the reference broad-crested weir without parapet wall, Configuration I ($L/h = 4/3$) and Configuration II ($L/h = 3.2$). The lowest discharge coefficients were observed at the highest upstream head and dimensionless discharge conditions, and Configuration II tended to produce smaller discharge coefficients than Configuration I for all flow conditions. The downstream depth d_2 data presented a similar trend. All the data indicated that the downstream flow was supercritical, i.e., $d_2 < d_c$, for all flow conditions.

The dimensionless discharge coefficient C_D of each weir configuration was deduced from the measured water discharge and upstream head above the broad crest by rearranging the standard weir equation as follows:

$$C_D = \frac{q}{\sqrt{g \times \left(\frac{2}{3} \times (H_1 - P)\right)^3}} \tag{2}$$

The present discharge coefficient data for all configurations are presented in Fig. 5(b). For the broad-crested weirs with dual-parapet walls, the discharge coefficient data fluctuated with the different flow patterns, yielding some seesaw appearance for flow conditions around the thresholds of the changes in flow regimes (Fig. 4). Despite the apparent scatter, the discharge coefficient data showed a consistent trend for all three configurations. That is, the largest discharge coefficients were seen for the reference broad-crested weir and the lowest discharge coefficients for Configuration II, i.e., a flat crest with relatively short dual-parapet walls: $L/h = 3.2$. For the entire data set of the reference broad-crested weir, the discharge coefficient was in average $C_D \approx 0.98$. For comparison, the mean discharge coefficient was $C_D \approx 0.91$ and 0.86 for broad-crested weirs with dual-parapet walls corresponding to Configurations I and II, respectively (tall and short parapet walls, respectively).

Energy dissipation across the tested structures increased significantly with the addition of dual parapet walls. The rate of energy dissipation was derived from the measured flow rate, upstream depth, and downstream depth for all configurations as follows:

$$\frac{\Delta H}{H_1} = \frac{H_1 - H_2}{H_1} \tag{3}$$

where H = total head; and subscripts 1 and 2 = upstream and downstream flow properties.

The data sets (not shown) presented some spread linked to the different flow regimes for the flat-crested weirs equipped with dual-parapet walls. Energy loss over the reference broad-crested weir without parapet walls was small for $d_c/L > 0.1$, as documented for broad-crested weirs with rounded corners (Henderson 1966; Bos 1976). With parapet walls, much more significant energy dissipation was observed, mostly (1) between the parapet walls through wave breaking and turbulent recirculatory motion in the cavity, and (2) at nappe impact downstream from the downstream parapet wall.

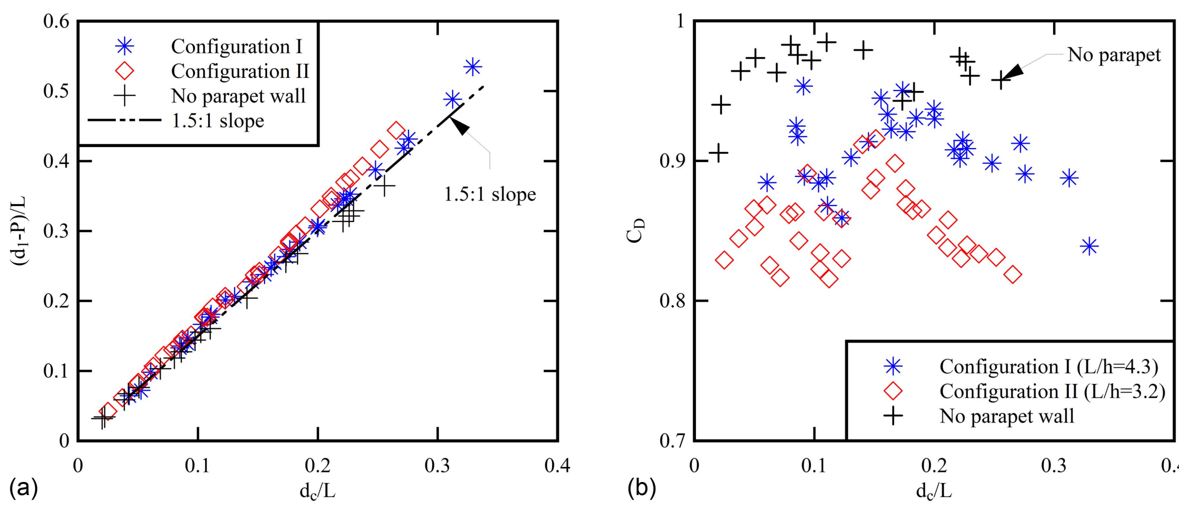

Fig. 5. Overflow characteristics of broad-crested weir with and without dual-parapet walls: (a) upstream water depth d_1; and (b) dimensionless discharge coefficient C_D as functions of the dimensionless discharge d_c/L.

Table 2. Digital video movies and flow conditions

Geometry	h (m)	L (m)	Q (m^3/s)	d_c/L	Movie filename	Camera and lens	Description
Configuration I	0.091	0.387	0.0075	0.085	IMGP5631.mov	Pentax K-3 and Voigtlander (Nakano, Japan) Nokton 58-mm f1.4 lens	Undular flow between dual-parapet walls; 4K movie [30 frames per second (fps)]. Run UQV1_0052 with red dye injection
			0.020	0.164	IMG_1826.mov	Apple iPhone XI	Top view of oscillating hydraulic jump between parapet walls; 1,080 px (30 fps). Run UQV1_0036
			0.020	0.164	IMGP4738.mov	Pentax K-3 and Pentax D-FA21-mm f2.4 lens	Side view of oscillating hydraulic jump between parapet walls; 4K movie (30 fps). Run UQV1_0036
			0.0265	0.198	IMGP5641.mov	Pentax K-3 and Voigtlander Nokton 58-mm f1.4 lens	Deflected jet flow above downstream parapet wall; 4K movie (30 fps). Run UQV1_0053 with red dye injection
Configuration II	0.121	0.392	0.0055	0.068	IMGP5522.mov	Pentax K-3 and Voigtlander Nokton 58-mm f1.4 lens	Undular flow between parapet walls; 4K movie (30 fps). Run UQV2_0042 with red dye injection
			0.0166	0.143	IMGP5550.mov	Pentax K-3 and Voigtlander Nokton 58-mm f1.4 lens	Deflected jet flow above downstream parapet wall; 4K movie (30 fps). Run UQV2_0043 with red dye injection
			0.0388	0.252	IMGP5173.mov	Pentax K-3 and Voigtlander Nokton 58-mm f1.4 lens	Thick-crested weir overflow motion; 4K movie (30 fps). Run UQV2_0018

Note: d_c = critical flow depth, where $d_c = [q^2/(g)]^{1/3}$; h = parapet wall height; L = crest length; Q = discharge; px = pixels; and 4 K = horizontal display resolution of approximately 4,000 pixels.

Conclusion

The present study investigated the effects of dual-parapet walls on the hydraulic flow patterns and discharge capacity characteristics of dam spillways equipped with a flat crest. Physical measurements were undertaken with three configurations: a reference broad-crested weir without parapet wall and two configurations with dual-parapet walls. Both qualitative and quantitative observations demonstrated some dramatic difference in terms of the overflow patterns and properties over these significantly different structures. On a flat crest with parapet walls, the flow patterns were more complicated and a range of different flow features was observed and documented, together with some strong flow recirculation in the cavity between the dual-parapet walls. Energy dissipation upstream from the first parapet wall and between the two parapet walls caused the parapet wall structures to be less efficient than the reference broad-crested weir. The installation of parapet walls reduced the discharge capacity of the broad-crested weir by 7% to 12% in average.

Altogether, this preliminary study demonstrated the complicated flow patterns above a flat-crested dam spillway equipped with dual-parapet walls. The present results deliver new pieces of information for the dam safety community, with better discharge coefficient information for the overflow sections with dual-parapet walls. Further research could explore more parameters, including the parapet height, thickness and crest shape, as well as other aspects of the base broad-crested weir shapes.

Appendix. Movies of Broad-Crested Weir Overflow

Visual observations of broad-crested weir overflows were conducted for three configurations in two channels with smooth horizontal invert and glass sidewalls. Each flume test section was 3 m long and 0.4 m wide. The sidewalls were 0.40 m high and made of transparent glass. The broad-crested weir was installed at 1.13 m downstream of the start of the glass-sidewalled test section. The test section ended onto an overfall, guiding the supercritical outflow. Two configurations corresponded to a broad-crested weir with dual-parapet walls, whereas the third one corresponded to the reference broad-crested weir (Table 1). Their description and the corresponding flow conditions are listed in Table 2.

Data Availability Statement

Some or all data, models, or code that support the findings of this study are available from the corresponding author upon reasonable request.

Acknowledgments

The author would like to thank Dr. John Macintosh, Water Solutions (Australia), Ms. Kok Keng Tan, Arup (Australia), and Dr. Tony Wahl, US Bureau of Reclamation (US) (in alphabetical order) for helpful comments and suggestions. He thanks Brett Bennett and Josh Clark, Tasmania Irrigation (Australia), for assistance in visiting and relevant information on the Meander Dam. He further thanks his spouse, Ms. Ya-Hui Chou, for her assistance with the field visits of the Paradise Dam, Wyaralong Dam, and Meander Dam. The author acknowledges the technical assistance of Jason Van Der Gevel and Stewart Matthews (University of Queensland, Australia).

J. Irrig. Drain Eng., 2025, 151(3): 06025001

Notation

The following symbols are used in this paper:

B = channel width (m), where $B = 0.40$ m in the present study;
C_D = dimensionless discharge coefficient;
D_H = hydraulic diameter (m), where $D_H = 4 \times A/P_w$;
d = water depth (m);
d_c = critical flow depth (m);
d_1 = inflow depth (m);
d_2 = downstream flow depth (m);
g = gravity acceleration (m/s^2), where $g = 9.794$ m/s^2 in Brisbane, Australia;
H = total head (m);
H_1 = upstream total head (m);
H_2 = downstream total head (m);
h = vertical parapet wall height (m);
L = broad-crest length (m);
P = weir crest elevation (m);
P_w = wetted perimeter (m);
Q = water discharge (m^3/s);
q = water discharge per unit width (m^2/s): $q = Q/B$;
Re = Reynolds number defined in terms of the mean velocity and hydraulic diameter, where $\mathrm{Re} = \rho \times [(V \times D_H)/\mu]$;
r = radius of curvature (m);
t = parapet wall thickness (m);
V = velocity (m/s);
V_c = critical flow velocity (m/s), where $V_c = (g \times Q/B)^{1/3}$;
V_1 = inflow velocity (m/s);
x = longitudinal distance (m) positive downstream;
z = normal distance (m) measured perpendicular to and above the channel invert;
z_o = invert elevation (m);
ΔH = total head difference (m);
Δz_o = drop in invert elevation (m);
μ = dynamic viscosity (Pa.s) of water; and
ρ = water density (kg/m^3).

Subscripts

c = critical flow conditions;
1 = upstream flow properties; and
2 = downstream flow properties.

Supplemental Materials

The supplemental movies are available online in the ASCE Library (www.ascelibrary.org).

References

Ackers, P., W. R. White, J. A. Perkins, and A. J. M. Harrison. 1978. *Weirs and flumes for flow measurement*. Chichester, UK: Wiley.

Bos, M. G. 1976. *Discharge measurement structures*. Publication No. 161. Delft, Netherlands: Delft Hydraulic Laboratory.

Bresse, J. A. 1868. *Cours de Mécanique Appliquée Professé à l'Ecole Impériale des Ponts et Chaussées. ('Course in Applied Mechanics lectured at the Pont-et-Chaussées Engineering School.')* [In French.] 2nd ed. Paris: Gauthier-Villard.

BSI (British Standard Institution). 1943. *Flow measurement*. BS 1042:1943. London: BIS.

Chanson, H. 1994. "Hydraulics of skimming flows over stepped channels and spillways." *J. Hydraul. Res.* 32 (3): 445–460. https://doi.org/10.1080/00221689409498745.

Chanson, H. 1995. *Flow characteristics of undular hydraulic jumps. Comparison with near-critical flows*. Rep. No. CH45/95. Brisbane, Australia: Dept. of Civil Engineering, Univ. of Queensland.

Chanson, H. 1996. "Free-surface flows with near-critical flow conditions." *Can. J. Civ. Eng.* 23 (6): 1272–1284. https://doi.org/10.1139/l96-936.

Chanson, H. 2004. *The hydraulics of open channel flow: An introduction*. 2nd ed. Oxford, UK: Butterworth-Heinemann.

Chanson, H. 2024. "Low-head hydraulic structures in irrigation and drainage engineering: Challenging operation and design implications." *J. Irrig. Drain. Eng.* 150 (5): 03124001. https://doi.org/10.1061/JIDEDH.IRENG-10288.

Chanson, H., and H. Wang. 2013. "Unsteady discharge calibration of a large V-notch weir." *Flow Meas. Instrum.* 29 (Mar): 19–24. https://doi.org/10.1016/j.flowmeasinst.2012.10.010.

Duncan, J. H. 1983. "The breaking and non-breaking wave resistance of a two-dimensional hydrofoil." *J. Fluid Mech.* 126 (Jan): 507–520. https://doi.org/10.1017/S0022112083000294.

Gonzalez, C. A., and H. Chanson. 2007. "Experimental measurements of velocity and pressure distribution on a large broad-crested weir." *Flow Meas. Instrum.* 18 (3–4): 107–113. https://doi.org/10.1016/j.flowmeasinst.2007.05.005.

Govinda Rao, N. S., and D. Muralidhar. 1963. "Discharge characteristics of weirs of finite-crest width." *Houille Blanche* 18 (5): 537–545. https://doi.org/10.1051/lhb/1963036.

Henderson, F. M. 1966. *Open channel flow*. New York: MacMillan Company.

Hotchkiss, R. H. 2001. "Flow over a "killer" weir design project." *J. Hydraul. Eng.* 127 (12): 1022–1027. https://doi.org/10.1061/(ASCE)0733-9429(2001)127:12(1022).

Isaacs, L. T. 1981. *Effects of laminar boundary layer on a model broad-crested weir*. Research Rep. No. CE28. Brisbane, QLD, Australia: Univ. of Queensland.

Leutheusser, H. J., and W. M. Birk. 1991. "Downproofing of low overflow structures." *J. Hydraul. Eng.* 117 (2): 205–213. https://doi.org/10.1061/(ASCE)0733-9429(1991)117:2(205).

Lin, J. C., and D. Rockwell. 2001. "Organized oscillations of initially turbulent flow past a cavity." *AIAA J.* 39 (6): 1139–1151. https://doi.org/10.2514/2.1427.

Morris, H. M. 1968. *Hydraulics of energy dissipation in steep, rough channels. Bulletin No. 19*. Blacksburg, VA: Virginia Polytechnic Institute.

Mossa, M. 1999. "On the oscillating characteristics of hydraulic jumps." *J. Hydraul. Res.* 37 (4): 541–558. https://doi.org/10.1080/00221686.1999.9628267.

Novak, P., V. Guinot, A. Jeffrey, and D. E. Reeve. 2010. *Hydraulic modelling: An introduction*. London: CRC Press, Taylor & Francis.

Novak, P., A. I. B. Moffat, C. Nalluri, and R. Narayanan. 1996. *Hydraulic structures*. 2nd ed. London: E & FN Spon.

Rouse, H. 1938. *Fluid mechanics for hydraulic engineers*. New York: McGraw-Hill Publication.

USBR (US Bureau of Reclamation). 1965. *Design of small dams*. 1st ed. Denver: US Department of the Interior.

Zhang, G., and H. Chanson. 2016. "Hydraulics of the developing flow region of stepped spillways. I: Physical modeling and boundary layer development." *J. Hydraul. Eng.* 142 (7): 8. https://doi.org/10.1061/(ASCE)HY.1943-7900.0001138).

J. Irrig. Drain Eng., 2025, 151(3): 06025001